EUROPEAN ORGANIZATION FOR NUCLEAR RESEARCH

CERN/SPSC 84-95
SPSC/P93 Add.3
December 1st 1984

PROPOSAL TO IMPROVE THE PERFORMANCE OF THE UA2 CENTRAL DETECTOR

The UA2 Collaboration

Bern[1], Cambridge[2], CERN[3], Milan[4], Orsay[5], Pavia[6], Pisa[7]

R.Ansorge[2], P.Bagnaia[3], M.Bonesini[4], C.Booth[2], K.Borer[1], M.Borghini[3], G.Carboni[7-3], D.Cavalli[4], V.Cavasinni[7], J-C.Chollet[5], A.G.Clark[3], C.Conta[6], G.Costa[4], P.Darriulat[3], T.Del Prete[7], L.Di Lella[3], K.Einsweiler[3], R.Engelmann[3], J-P.Fabre[3], L.Fayard[5], M.Fraternali[6], D.Froidevaux[5], J-M.Gaillard[5], O.Gildemeister[3], V.G.Goggi[6], C.Goessling[3], B.Hahn[1], H.Haenni[1], J.R.Hansen[3], P.Hansen[3], N.Harnew[3], E.Hugentobler[1], L.Iconomidou[5], P.Jenni[3], S.Katvars[2], M.Livan[6], B.de Lotto[5], L.Mandelli[4], L.Mapelli[3], M.Mazzanti[4], K.Meier[3], B.Merkel[5], R.Moning[1], M.Moniez[5], M.Morganti[7], D.Munday[2], C.Onions[3], M.A.Parker[3], G.Parrour[5], F.Pastore[6], L.Perini[4], J-P.Repellin[5], A.Rimoldi[6], J.Rushbrooke[2], J.Schacher[1], F.Stocker[1], M.Swartz[3], S.Tovey[3], W.Tsang[2], M.Valdata-Nappi[7], V.Vercesi[6], A.Weidberg[3], T.White[2].

1. INTRODUCTION

A proposal to improve the performance of the UA2 detector (CERN/SPSC 84-30, SPSC/P93 Add.2) was recently submitted to the SPS Committee. A number of choices were presented, which were dictated by the following considerations:

i) The upgraded UA2 must be operational in 1987, as soon as the Collider resumes operation, in order to maximise its physics output during the period when TEV 1, with nearly three times as high a c.m. energy, has not yet taken over leadership.

ii) The upgraded UA2 must remain competitive on the major physics issues rather than diversify its detection capabilities.

iii) Priority is given to improve the quality of the missing transverse energy measurement.

iv) Modifications to the vertex detector aim at ensuring that multivertex events can be reconstructed and at improving the detector performance in relation to electron identification.

These general considerations were received favourably by the SPS Committee and, at their 69th meeting, the Research Board approved the proposed end-caps in a first stage. At the same time they urged us to come up as soon as possible with a definitive design of the central detector: the present document answers this request.

The main components of the proposed central detector were listed in a recent document (CERN/SPSC 84-86, SPSC/M395). Moving outwards from the interaction region they include (Figure 1):

i) A small diameter beryllium vacuum chamber to be installed in 1985,

ii) A jet chamber vertex detector (JVD) providing an accurate measurement of the longitudinal and transverse positions of the event vertex,

iii) A matrix of silicon counters with the double purpose of measuring ionisation and helping in pattern recognition,

iv) A pair of transition radiation detectors (TRD) providing an additional rejection factor of at least an order of magnitude against fake electrons,

v) A multilayer scintillating fibre detector (SFD) for tracking and for measuring early electromagnetic showers developing after a 1.5 radiation length thick converter.

The proposed design is expected to substantially reduce the two most significant sources of backgrounds faking electrons: converted photons from π^0 decays and narrow π^0-charged hadron pairs (overlaps).

Converted photons are a potential background when the conversion occurs in front of or within the JVD: conversions occuring at larger radii are recognised as such from the absence of an associated track in the JVD. Early conversions include π^0 Dalitz decays and external conversions in the vacuum pipe and inner chamber wall (0.5% of a radiation length in total, 4 times less than in the present detector). They are strongly reduced by the requirement of a low ionization energy loss in the JVD and silicon array.

In the present design, overlaps contribute about 50% of the background faking electrons at transverse momenta between 15 and 25 GeV/c. At lower transverse momenta, where jet fragments are less collimated, single hadrons interacting in the preshower converter are an additional significant source of background. In both cases a rejection factor of at least an order of magnitude is expected from the TRD.

These new features contribute important improvements to the performance of UA2 in searches for events containing electrons and they improve electron identification at transverse momenta populated by heavy flavour semileptonic decays, in particular from $W \rightarrow t\bar{b}$.

The insertion of a transition radiation detector, a key feature of the proposed design, is at the price of dedicating to it a major fraction of the space available in the central region of UA2 (about half of the radial range). In turn this implies very efficient and compact tracking devices fitting in the remaining available space: the JVD and silicon array in the inner region, the SFD in the outer region. Both have the ability to measure track segments. In addition the outer cathodes of the TRD chambers are equipped with strips to help match the two regions.

While inner tracking provides direct localisation in space (charge division on the JVD wires and silicon pads), the SFD measures three stereoscopic projections. The stereo angle has been chosen small enough to reduce ghost tracks to a satisfactory level while retaining sufficient localisation accuracy. The outer layers of the SFD act as a preshower counter, thus providing a compact and unified design in the angular range covered by the central UA2 calorimeter. Modifications to the design of the extreme electromagnetic calorimeter cells have been necessary to enlarge the space available for the UA2 central detector.

The overall dimensions of the UA2 central detector have been defined to match the geometry of the central and end cap calorimeters and to provide tracking capability over the solid angle in which electrons are to be identified. This implies complete coverage in azimuth (Φ) and a polar angle (θ) coverage from 25° to 155° allowing for vertex excursions of ±200 mm along the beam direction (z). This latter constraint is forced on us by the geometry of the central calorimeter. While it is perfectly adequate in the present mode of Collider operation it would become too small if longer bunches were used as the result of a modification of the RF system.

The UA2 central detector will be supported from the central calorimeter and the various cables (≅600 cm^2 in cross-section) connected

to its end plates are channelled to the UA2 cable-rails through the space between the central and end-cap calorimeters.

In what follows we describe each component of the proposed detector, their expected performance and the results of prototype measurements. We also evaluate the construction time table and the cost and we specify the responsibilities of each of the collaborating Institutes.

2. VACUUM CHAMBER

A beryllium vacuum pipe with 62.8 mm outer diameter and 0.9 mm thickness has been designed by the SPS Division (8095-2802-1/B) and will be installed in LSS4 in time for the 1985 running period. Compared with the present corrugated stainless steel vacuum pipe it gives an additional radial space of 35 mm and increases the transparency, measured in radiation lengths, by about a factor 5.

3. JET CHAMBER VERTEX DETECTOR (JVD)

The design of the JVD, constrained to fit between the vacuum pipe (R = 32 mm) and the silicon array (R = 140 mm), is of the jet chamber type in order to satisfy the following requirements:

i) to measure space points in order to minimize ambiguities in the event reconstruction;

ii) to sample at least 12 space points per track with $\leq$ 150 μm accuracy in $R \times \Phi$;

iii) to separate nearby tracks in projection: $R \times \Delta\Phi \leq 1$ mm ;

iv) to provide good accuracy in z, both to separate double vertices and to allow precise extrapolation to the outer tracking devices;

v) to minimize photon conversions, implying a good transparency.

Longitudinal and transverse cross-sections are shown in Figures 2 and 3. The detector has an outer radius of 135 mm, an inner radius of 35 mm, and a total length of 1600 mm (excluding the electronics). The chamber is divided into 16 azimuthal sectors, each equipped with 13 (staggered) sense wires 1100 mm long at 6.5 mm spacing, with guard wires interspersed among them (Fig. 4). Tracks will be measured down to $\theta = 25^{\circ}$, with allowance for $\pm$ 200 mm excursions of the vertex along the beam. To minimize the material between the beam and the sensitive region, only the external cylindrical wall will carry the mechanical tension of the wires. Digitization of the drift time and readout of the z coordinate by charge division will be provided by the 100 MHz Flash-ADC (FADC) system developed at CERN by F. Bourgeois [1]. A summary of the relevant parameters is given in Table 1.

To enhance two-track separation capability we plan to operate the chamber with a "slow" gas (90% CO_2 + 10% Isobutane), at a drift velocity $\approx$ 1cm/μs (E/P = 1.3 kV/cm/atm). Using CO_2, the NA34 experiment has reported a 600 μm two-track separation [2]. Studies by the OPAL group [3] have shown that 100 MHz FADC's can resolve chamber pulses at Δt = 80 ns, corresponding in our case to a 800 μm two-track separation. The main problems will arise from the spread in drift velocity due to the cell geometry and to inhomogeneities of the electric field. The performance of the chamber has been studied using a Monte Carlo simulation of the charge collection process taking into account the detailed geometry of the electric field [4]. We find that a two-track separation of 1 mm can be achieved, with an accuracy of 150 μm in R$\times\Phi$.

The precision σ_z of the charge division method ranges between 0.3% and 1% of the total wire length, mainly depending on the signal/noise ratio [5]. We may wish to improve this ratio by operating the detector

up to 4 ata (atm absolute). To avoid stresses due to the pressure on the end plates holding the wires, the chamber will be enclosed in a pressure vessel, and the signals and HV's will be brought outside using gas-tight feed-throughs. The beam pipe (0.9 mm thick Be) will form the inner wall of the vessel itself. For 4 ata operation the vessel outer wall could be made from 1.5 mm aluminum or from a carbon-fibre based sandwich, to minimize the thickness measured in radiation lengths.

To improve the accuracy of the track extrapolation to the SFD ($R \cong 400$ mm), a cathode readout of the outermost sense wires using 168 cylindrical strips perpendicular to the beam direction measures the z-coordinate of the avalanches on every sense wire (Fig. 5). The strips will be supported from the outer cylindrical wall of the chamber, which will also incorporate the field shaping electrodes and the lines to bring the strip signals outside towards the end plates. Each cathode strip will be read by a FADC, in order to associate in time the cathode and wire measurements. From the performance of the strip chambers C_1-C_4 used presently in UA2 we expect a precision (averaged over all tracks) $\langle\sigma_z\rangle \approx 700$ μm. Notice that, with respect to C_1-C_4, the occupancy of the strips in this design is diluted by a factor $f = T_d/\Delta T$, where ΔT (≈ 200 ns) is the integration time of the signal on the strip and T_d (≈ 2.5 μs) is the maximum drift time of the cell: $f \cong 12$. The dead space then remains small even in the case of very high multiplicity events or in the case of event pile-up.

4. SILICON ARRAY

4.1 Introduction

On a cylinder of radius 140 mm around the beam pipe, we intend to construct a matrix of 432 silicon counters, each divided into seven individual readout channels (3024 in total). This array is immediately outside the JVD. It will be used in conjunction with that detector to:

i) reject photon conversions by providing, with good granularity, a measurement of the ionisation of charged tracks, and

ii) help track reconstruction by providing a space-point measurement.

It is intended to install this array before the 1985 data taking period and it has therefore been designed to be also compatible with the existing vertex detector.

4.2 Mechanical arrangement

Each silicon counter is of size 61×40×0.3 mm^3, nine of them being arranged on each of 48 fibreglass boards, and each board covering an azimuthal interval of 15° and half the polar angle range. By overlapping individual counters the array has a negligible inactive area. On each board low noise amplifiers are mounted behind the detectors, and the signals are subsequently transferred to the end of the detector via a multi-layer circuit board. Shaping amplifiers, track-and-hold circuits and multiplexing electronics are mounted at the end of each board. Each board is enclosed in a box and mounted on a thin support cylinder as shown in Figure 6. Table 2 lists the dimensions of the silicon array and its thickness measured in radiation lengths.

Prototype counters of the final design specification have already been manufactured [6] and, as described below, extensive tests are in progress. A prototype board of three counters has been constructed for tests in the UA2 apparatus during the 1984 run (Figure 7), to gain experience with counter stability, electronic noise, etc.

4.3 Electronics

Because of the environment of the silicon detector, and because of the large number of signal channels, extremely compact electronics is required. At the same time, however, the electronics must satisfy:

i) low noise at the preamplifier stage (≅ 1500 electrons rms at 150 pF input capacitance),

ii) negligible cross-talk,

iii) low cost, and

iv) short-term availability.

These requirements have led to the choice of a hybrid preamplifier mounted on the board directly behind the silicon. Prototype FET-input preamplifiers [7] are currently being tested. The signals (63 per board) are transferred via a separate multi-layer board to the end of the detector where hybrid shaping amplifiers ($\tau \cong 0.8\mu s$) are followed by a track-and-hold circuit. Prototype circuits already exist. The multiplexing and ADC stages must still be finalised.

4.4 Counter prototypes

Twelve prototype counters, of the final design specification [6], have been extensively tested, and the prototype tests are continuing. Tests which are underway include:

i) long-term leakage current tests,

ii) tests of pulse-height resolution using a Ru^{106} β-source,

iii) the dependence of the above on the applied bias voltage,

iv) radiation damage, including tests with a 1mCi Sr^{90} source, and with radiation in the SPS tunnel.

Typical pulse-height spectra for counters passing our design criteria are shown in Figure 8. A rejection factor against photon conversions of 15 to 20, with 90% efficiency, is expected.

Within the limited statistics of present radiation damage tests, the counter deterioration (measured as an increase in leakage current) is $\cong$ 1 nA/cm²/Gray in the UA2 environment; this suggests, for the present counter design, a maximum tolerable dose of $\cong$ 200 Gray. No problem is therefore expected, apart from possible accidental beam losses (the total dose during the 1983 running period was $\lesssim$ 3 Gray at the proposed array location).

Strict specifications have been imposed on the supply of silicon counters from the manufacturer [6], and acceptance tests, in particular concerning leakage current and pulse-height resolution, will be made on each of the supplied counters.

5. TRANSITION RADIATION DETECTOR (TRD)

The TRD is inserted in the 210 mm of radial space between the silicon array and the SFD. It is made of two modules, each consisting of a lithium radiator to emit X-rays and a xenon proportional chamber to detect them. The Orsay group which is taking the responsibility for designing and constructing this detector has already built and successfully operated two similar modules in the charged hyperon experiment at the SPS [8].

Each radiator is cylindrical and has a thickness of 80 mm. It contains a stack of 400 lithium foils, 40 μm thick , separated by 160 μm. The spacing is maintained by corrugations in the foils. The total lithium weight is 50 kg. The average number of photons produced by an electron of energy > 5 GeV traversing the radiator at normal

incidence and subsequently absorbed in the xenon chamber is 2. Their average energy is 6 keV.

The xenon chambers consist of two layers of gas, 10 and 6 mm thick, separated by a grid of wires connected to ground. The gas mixture is 70% xenon, 30% CO_2. In the first layer, a drift velocity of 20 μm/ns is obtained with an electric field of 400 V/cm. The second layer is used as an amplification stage. The signal wires are separated by 4.4 mm and interspersed with field wires (Fig.9). The signal wires are at a voltage of 1.6 kV and the two cathodes of the amplification stage are grounded. This allows the outer cathode to be made of helical strips from which the charge can be read out.

For safety reasons the radiators and the chambers will be enclosed in gas-tight containers and helium will be circulated inbetween the radiator foils.

The wires are connected to preamplifiers and the signals are measured in a 100 MHz FADC [1]. This allows the observation of the individual X-rays which are converted in the drift space with a time resolution of better than 100 ns and with a measurement of their energy. The X-ray signals are superimposed on the more uniform and much smaller contribution from ionization energy loss (dE/dx) of the primary electron. These features are successfully taken care of by cluster counting methods [9].

The strips are connected to preamplifiers and the integral of the charge induced by the avalanche is measured in ADC's. Since the signals coming from the drift space and the amplification stage arrive at different times, we plan to measure them independently.

The correlation between the charge collected on the wire and that induced on the strips gives a measurement of the coordinate along the beam of both the signal coming from the drift space (dominated by X-rays in the case of electrons) and the signal coming from the amplification stage (dominated by dE/dx from all ionizing tracks). This helps the identification of the electrons and can also be used in the overall reconstruction programme for all the ionizing tracks.

We have used a computer programme [10] to evaluate the electron detection efficiency and the rejection against hadrons, and to optimize the radiator and chamber parameters. The results of this programme have been compared to real test measurements. They show that a two-module design is more efficient than a single-module design given the available space. Using the cluster counting method, we expect a rejection of a factor 15 against hadrons with an efficiency of 80% for electrons. This performance improves by a factor 3 when the polar angle of the electron changes from 90° to 30°. The rejection is of course degraded when two ionizing particles hit the same wire but the measurement of the charge induced on the strip will help to recover part of this loss.

The dimensions and the number of channels of the chambers are given in Table 3. Each module is about 0.015 thick in both radiation length and interaction length.

6. SCINTILLATING FIBRE DETECTOR (SFD)

Recent developments in scintillating plastic fibres made at Saclay offer an attractive possibility to construct a compact position detector with good track reconstruction efficiency and adequate spatial accuracy. As emphasized above compactness is absolutely necessary to provide space within the UA2 apparatus for the TRD. The present design of the SFD is based upon:

i) extensive tests that we have made with fibres during the second half of 1984,

ii) Monte Carlo studies of the track reconstruction properties using simulated $p\bar{p}$ events,

iii) measurements on, and investigations of, the various components (image intensifiers, CCD, digitizers) necessary to read and digitize the fibre information.

6.1 Geometry and choices for the SFD

The SFD, whose general layout is shown in Figure 1, has a radial thickness of 60 mm at an average radius of 410 mm. It consists of about 60000 fibres, with a total length of 150 km, arranged in seven groups of three layers (triplets). In each triplet, the angles of the fibres with respect to the beam axis are $-\alpha$, 0, and α for the three layers respectively. This provides space coordinates from three stereoscopic projections. Within the angular range covered by the central UA2 calorimeter, a converter (1 and 0.5 radiation lengths respectively) is inserted in front of each of the two outer triplets, which are thus used as a preshower counter.

The choices for the design of the detector are based on the standard fibres which we have tested (see Appendix 1). They are made of a core of polystyrene, doped with POPOP and butyl-PBD, with a thin cladding ($\cong$10 μm) and have a numerical aperture of 0.62. These fibres are currently produced by Saclay (STIPE) in lengths of 600 m with a 1 mm diameter. Several considerations and measurements have led to the 1 mm choice:

i) A minimum ionizing particle passing through a 1 mm diameter fibre leads, on average, to 26 photons on each side, at 1 m distance from the impact point (see Appendix 1).

ii) For a typical amplifying and demagnifying optical system (see below), a point on the CCD front face may collect light from an input area of $\cong$ 300 μm diameter. This limits any benefit of using smaller fibres.

iii) The cladding has a thickness which is proportional to the fibre diameter and becomes more fragile for smaller diameters.

iv) The attenuation length, $\cong$2 m for a diameter of 1 mm, becomes shorter for smaller diameters.

We plan to view the fibres from one end only and to place a reflector at the other end. The expected efficiency per incident photon of the input stage of an image intensifier system is ≅ 10%. We expect on average 91% efficiency per fibre for particles at $\theta = 90°$. For other values of θ the average efficiency becomes closer to 100%.

The final optical readout system is not yet chosen. We will nevertheless indicate the arrangement foreseen for the fibres, which will be grouped into N = 40 to 50 azimuthal sectors. Adjacent sectors are read out from opposite ends to allow for more space at each readout station. Stereoscopy is arranged in such a way that all fibre layers converge to one of the N azimuthal sectors. This geometry implies that the stereo angle α should be a multiple of $\alpha_0 = 4\pi R/NL$, where R and L are the radius and the length of the fibre layer, respectively ($\alpha_0 \cong 3°$). A larger stereo angle implies better precision but more ambiguities in track reconstruction and hence more ghost tracks. From a Monte Carlo simulation the value $\alpha \cong 12°$ was chosen for the five triplets preceding the converter. In this part of the detector, the angular precisions of the track segments obtained in the transverse and longitudinal directions are $\sigma(\Phi) = 15$ mrad and $\sigma(\theta) = 30$ mrad respectively . The stereo angle α for the two triplets of the preshower section was chosen to be $\cong 24°$ in order to compensate for the smaller number of triplets while maintaining a good match between the angular measurement accuracies before and after the converter.

Control over possible changes of the distortions induced by the imaging system will be obtained using referénce fibres inserted among the scintillating fibres and illuminated by an external light source.

Tests concerned with the sensitivity to radiation of the various SFD components (fibres, image intensifiers, CCD) will be performed early next year using a prototype operated in the LSS4 environement.

6.2 Readout and digitization

A schematic representation of the system is shown in Figure 10. It is composed of three parts. The light output from the fibres is amplified with a photon gain of 10^4 by the image intensifiers (II). The light is then converted by a charge coupled device (CCD) into a signal which is read by the digitizer and stored in a memory. The photon gain of the II system is chosen such that the average signal per CCD element (pixel), within the area corresponding to a fibre hit by a charged particle, is ten times larger than the noise level of the CCD. The principle of operation is also indicated in Figure 10. The gate of the II system is normally open and information accumulates in the CCD. About 1 μs after each crossing an external trigger decision (not using the fibre information) leads to one of the two following sequences:

i) no-trigger case: a fast-clear pulse is applied to the CCD, draining away the accumulated charge in $\lesssim$ 1.5 μs. The II gate stays open and new information is collected in the CCD.

ii) trigger case: the gate on the II system is closed to prevent illumination from subsequent $p\bar{p}$ interactions while reading the CCD information related to the event associated with the trigger ($\cong$4 ms). When the CCD reading is completed the II gate is reopened.

We shall now describe in more detail the three parts of the system.

6.2.1-The image intensifier chains

An image intensifier consists of a photocathode, with fibre optic input, an electron accelerating stage (with or without multiplication) and a phosphor screen coupled to a fibre optic output. The time for light amplification is determined by the time constant of the particular phosphor used for the screen. The II chain of the proposed detector has to collect the light from fibre bundles, amplify with a photon gain of about 10^4 within a time of about 3 μs, and demagnify so that the output dimensions match the active area of the CCD (4.3×5.8 mm^2 for

the CCD we plan to use [11]). The chain must have the ability of being gated and must give a resolution corresponding to $\leq$ 300 μm FWHM at the fibre level.

From investigations with several firms [12], it has become clear that two amplifying stages are necessary to meet our gain specifications: a moderate gain unit and a high gain II tube with microchannel plate. To determine the components which can be used in an II chain we follow very definite guidelines:

i) a unit must correspond to a standard production tube with minimal modifications, such as a different photocathode material and a fast phosphor screen.

ii) the photon gain must be achieved while running the components at a safe voltage to ensure longevity. In particular for an II with a microchannel plate it implies the use of a 20% lower high voltage value than that specified by the constructor, thus lowering the photon gain by a factor $\cong$10.

iii) the photon gain of all possibly interesting II chains will be measured using our own test bench, which is already in operation and has been used to measure the gain of several II tubes.

Although we have not yet made a final choice of the II chain, we are confident that the required performance can be achieved in several ways. As an illustration, one of the systems under active study is shown in Figure 11. The 50 mm input diameter leads to the total number of II chains, N = 40 to 50, given above. We are also studying other possibilities with larger input diameters which would lead to a smaller number of (more expensive) II chains.

6.2.2-The charge coupled device (CCD)

The fibre optic taper at the exit of the II chain is directly coupled to a CCD where the light is converted to electrical charges which are stored. It is essential that unwanted information can be cleared off from the device during the time available between two $p\bar{p}$ crossings. This can be achieved by using the antiblooming system with which some commercial CCD's are equipped. In collaboration with the manufacturer [11], we have tested the CCD TH7852 which we plan to use, and we have found that it can be fast-cleared by applying a pulse of ≤ 1.5 μs duration to the antiblooming input.

The CCD TH7852 has an optical area of 5.8×4.3 mm² with 144×208 sensitive elements (pixels). Each pixel has an active area of 19×30 μm² and a geometrical area of 28×30 μm². With the demagnification of the II chain shown as an example in Figure 11, a 1 mm diameter fibre may illuminate up to about 20 pixels. Within the 4 ms time duration necessary to read the CCD information for an accepted event, the electrical noise at 25°C is 100 electrons per pixel. It is this noise level which leads to the required 10^4 photon gain of the II chain for a signal to noise ratio ≥ 10. If needed the CCD noise can be further reduced by operating at lower temperature (by a factor of 2 per 8°C).

6.2.3-Digitization of the information

For events satisfying the trigger requirement, the content of each CCD is read out. We consider that pulse height information is useful in pattern recognition, and necessary for the preshower part of the SFD. In addition, since in a typical event particle tracks cross $\cong 2\%$ of the fibres, the compaction of data is essential for an efficient and economical utilization of memory.

In the present tests we are using a Threshold Video Digitizer (TVD) developed at Cambridge, which digitizes information only from pixels whose signal exceeds a given threshold. The TVD output provides a 6 bit digitization of the pixel signal, which is stored temporarily in a buffer containing 16k words of memory and read out via CAMAC.

While this design is well-tested and satisfies our present needs, further development is required to reduce the amount of data to an acceptable level in the actual experiment.

6.3 Fibre development

The SFD design presented here is based on existing standard fibres produced at Saclay. It is obvious that increasing the light output of the fibres would improve the performance of the detector. For instance, by increasing the light output by a factor of 1.5, the average 91% efficiency per fibre for particles at $\theta = 90°$ (see section 6.1) would rise to 97%. A few tests and developments are already underway at Saclay (on new wave shifters, replacing POPOP by K27, or on new cladding materials with a lower refractive index, etc). We have defined in collaboration with Saclay a programme of developments and tests to be concluded within the next six months. This programme includes the production of batches ($\cong$ 600 m) of each fibre type and the measurement of their light output, attenuation length, sensitivity to radiation, etc, as well as tests in particle beams.

Based on the results of this programme, we shall then decide which type of fibre will be used in the actual detector design.

7. TIME TABLE AND COSTS

The vacuum chamber and the silicon array will be installed in UA2 in time for the 1985 data taking period. Similarly the FADC's of the JVD electronics will be used on the present UA2 jet chambers in 1985.

The main milestones of the rest of the upgrade programme concerning the UA2 central detector are given below:

i) JVD:

April 1985: Tests using a planar prototype chamber.

December 1985: Prototype JVD constructed and tested.
December 1986: Two JVD (including a spare) constructed and tested, ready for installation.

ii) TRD:

December 1985: Completion of tests related to the detailed design of the radiators and chambers.
December 1986: TRD constructed and tested, ready for installation.

iii) SFD:

June 1985: Completion of fibre development tests.
September 1985: Completion of prototype II tests and final orders.
July 1985 to July 1986: Final design and construction of the detector.
July 1986: Completion of tests and assembly of the II chains.

Cost estimates for the different parts of the upgraded UA2 central detector are listed in Table 4.

The responsibilities of the Institutes collaborating in the UA2 upgrade effort are as follows:

i) Calorimeter end caps: CERN and Milan,

ii) End-cap calorimeter preshower counters: Bern and Pavia,

iii) JVD: Pisa,

iv) Silicon array: CERN and Bern (for electronics development),

v) TRD: Orsay,

vi) SFD: Cambridge, CERN and Saclay.

The contribution of Saclay (M.Bourdinaud, M.Thevenin and collaborators) to the project is presently restricted to the research and development phase of the detector design. We are having contacts with Saclay in the hope that a larger group of physicists would participate.

ACKNOWLEDGEMENTS

We are deeply indebted to P.Jarron, D.Perrin, P.Rancoita, and P.Sonderegger for help and advice.

Appendix 1: Measurement of the fibre photon yield

We have performed a measurement of the light yield produced by minimum ionizing particles traversing 1 mm diameter scintillating fibres manufactured at Saclay. The fibres were exposed to a 3 GeV pion beam at the CERN PS and the light was measured using phototubes having ≅20% photocathode efficiency in the relevant spectral range. To get an idea of typical fibre to fibre fluctuations, a set of fifty fibres, each 1 m long, was studied. The fibres were positioned with an accuracy of ≅100 μm, parallel to each other in five horizontal layers of ten fibres each. The distance between adjacent layers and the distance between adjacent fibres of the same layer were both 2 mm, thus avoiding cross talk effects which might be present in a tight bundle. While a single phototube was used to collect the total light from the fifty fibres at one end, ten independent phototubes were used at the other end, each viewing one and only one fibre of each horizontal layer. The whole fibre set could be moved vertically with a setting accuracy of ≅10 μm, thus allowing for scanning each fibre layer across a pencil beam defined by two scintillators with a vertical width of 500 μm, located in the beam line on either side of the array.

The pulse height spectra from each phototube were recorded and analysed in terms of a pedestal and of a continuous distribution to obtain, for each fiber, the probability of having zero photoelectrons. For the optimum position of the fibre layers with respect to the beam, typical inefficiencies of $\lesssim 1\%$ were obtained, corresponding to a mean number of 5.0 photoelectrons per fibre assuming Poisson statistics. An independent measurement using neutral density filters inserted between the fibre ends and the photocathode gives a value of 5.3 for the same number. Once the effects of light attenuation in the fibre (≅60 cm path), of photocathode efficiency (≅20%) and of geometry are taken into account, the mean number of photons collected after 1 m of fibre is therefore 26 ± 2.

REFERENCES

1. F. Bourgeois, Nucl.Inst.Meth. 219(1984)153, F. Bourgeois et al., CERN/EF 84-14, Oct 1984.

2. OPAL Technical report , pp. 58 and ff.

3. D. Bettoni et al., CERN-EP/84-162, 29 November 1984.

4. Courtesy of J. Va'vra (SLAC).

5. V. Radeka, IEEE Trans. Nucl. Sci., NS-21,nr 1(1974)51.

6. Micron Semiconductor Ltd, Lancing,Sussex,United Kingdom.

7. Laben electronics, Milan,Italy, Mod.5254.

8. M.Bourquin et al., Nucl. Inst. Meth. 204(1983)311; see also W.Willis in Proc. Yerevan Conf. on transition radiations,1977.

9. C.W.Fabjan et al., Nucl. Inst. Meth. 216(1983)105.

10. Courtesy of B.Dolgoshein and I.Gavrilenko; see also NA32 proposal.

11. Thomson-CSF, CCD TH7852.

12. DEP, Roden,Holland; ITL, St.Leonards-on-sea,UK; ITT, Fort Wayne,Ind.,USA; Philips, Eindhoven,Holland; Proxitronic, Bensheim,Germany;Thomson-CSF, Boulogne-Billancourt,France; Westinghouse, Horsehoads,New York,USA;

TABLE 1

JET VERTEX DETECTOR

Main parameters

Total length (incl. vessel)	1600	mm
Inner Radius	34.75	mm
Outer Radius	135	mm
Sensitive length	1100	mm
Inner sensitive radius	38.25	mm
Outer sensitive radius	122.75	mm
Number of cells	16	
Number of sense-wires/cell	13	
Sense wire spacing	6.5	mm
Sense wires staggering	0.15	mm
Total number of sense-wires	208	
Total number of field-wires	832	
Total number of cathode strips	168	
Strip spacing	5 to 15	mm
Total number of FADC channels	584	

Thicknesses

	(mm)	(r.l.)
Be pipe	1.0	0.3 %
Inner wall	0.4	0.2 %
Outer wall	1.0	0.5 %
Vessel (aluminum)	1.5	1.7 %
Vessel (carbon fibre)	1.0	0.5 %

TABLE 2

SILICON ARRAY

Dimensions

Radius	140-168 mm
Active length	1100 mm
Total length	1820 mm

Quantities

Number of channels	3024
Number of counters	432
Number of boards	48

Thicknesses

Material	rad. l.
Silicon	0.3%
Board	0.5%
Preamplifier and readout	0.7%
Assembly box	0.5%
Support cylinder	0.1%

TABLE 3

TRD parameters

	Radius	Length	Nr(wires)	Nr(strips)
Chamber 1	265	1600	384	512
Chamber 2	370	1880	528	704
			912	1216

TABLE 4: COST ESTIMATE

JVD:	
Mechanics	100 kSF
600 channels of FADC	300 kSF
Preamplifiers	15 kSF
HV system	25 kSF
Cables	10 kSF
Subtotal	450 kSF
SILICON ARRAY:	
Silicon detectors	170 kSF
Mounting boards, readout, etc	10 kSF
Preamplifiers	85 kSF
Mechanics	25 kSF
Shaping amplifiers, multiplexers	100 kSF
ADC's, power supplies, etc	75 kSF
Sundry items (test facilities, etc)	25 kSF
Subtotal	490 kSF
TRD:	
Mechanics	100 kSF
Lithium	100 kSF
Gas	80 kSF
920 channels of FADC	460 kSF
ADC's	120 kSF
Pre amps	100 kSF
Subtotal	960 kSF
SFD:	
Scintillating fibres	45 kSF
Image intensifiers	1200 kSF
CCD's	60 kSF
Digitizers	200 kSF
Mechanics	200 kSF
Subtotal	1705 kSF
GRAND TOTAL	3605 kSF

FIGURE CAPTIONS

1. The proposed central detector: schematic layout.

2. Longitudinal cross-section of the JVD. 1: beryllium pipe; 2: pressure vessel; 3: outer chamber wall; 4: inner chamber wall; 5: end plates for wire support; 6: signal and HV feed-throughs.

3. Schematic transverse cross-section of the JVD. 1: beryllium pipe; 2: pressure vessel; 3: outer chamber wall; 4: inner chamber wall.

4. Layout of the basic JVD cell. 1: sense wire; 2: guard wire; 3: field wire; 4: outer chamber wall (supporting the strip readout); 4: outer vessel wall.

5. Layout of the JVD cathode-strip readout. 1: sense wires; 2: cathode strips; 3: readout lines.

6. The silicon array: detailed cross-section.

7. Prototype silicon counters: a) Prototype board (1/3 length) with three silicon counters mounted. The two counters on the right are of the final dimensions. b) Reverse side of prototype board showing preamplifiers (similar performance to final design), and the multi-layer readout board.

8. Pulse height spectra of two silicon prototype detectors (bias voltage of -60 V, Ru^{106} source, resolutions given in percent of minimum ionizing particle response, resolution of signal peak evaluated from half width at half maximum). Pedestal widths are measured in percent of the peak pulse-heights.

9. Cross-section of the inner TRD module showing the lithium radiator and the xenon chamber. The thin window on the chamber side is coated with graphite to define the cathode potential in the drift space.

10. Principle of operation of the readout and digitization system of the SFD.

11. An example of an image intensifier chain. The photon gains (G) of each element are given, taking into account the coupling losses. The second intensifier uses a microchannel plate.

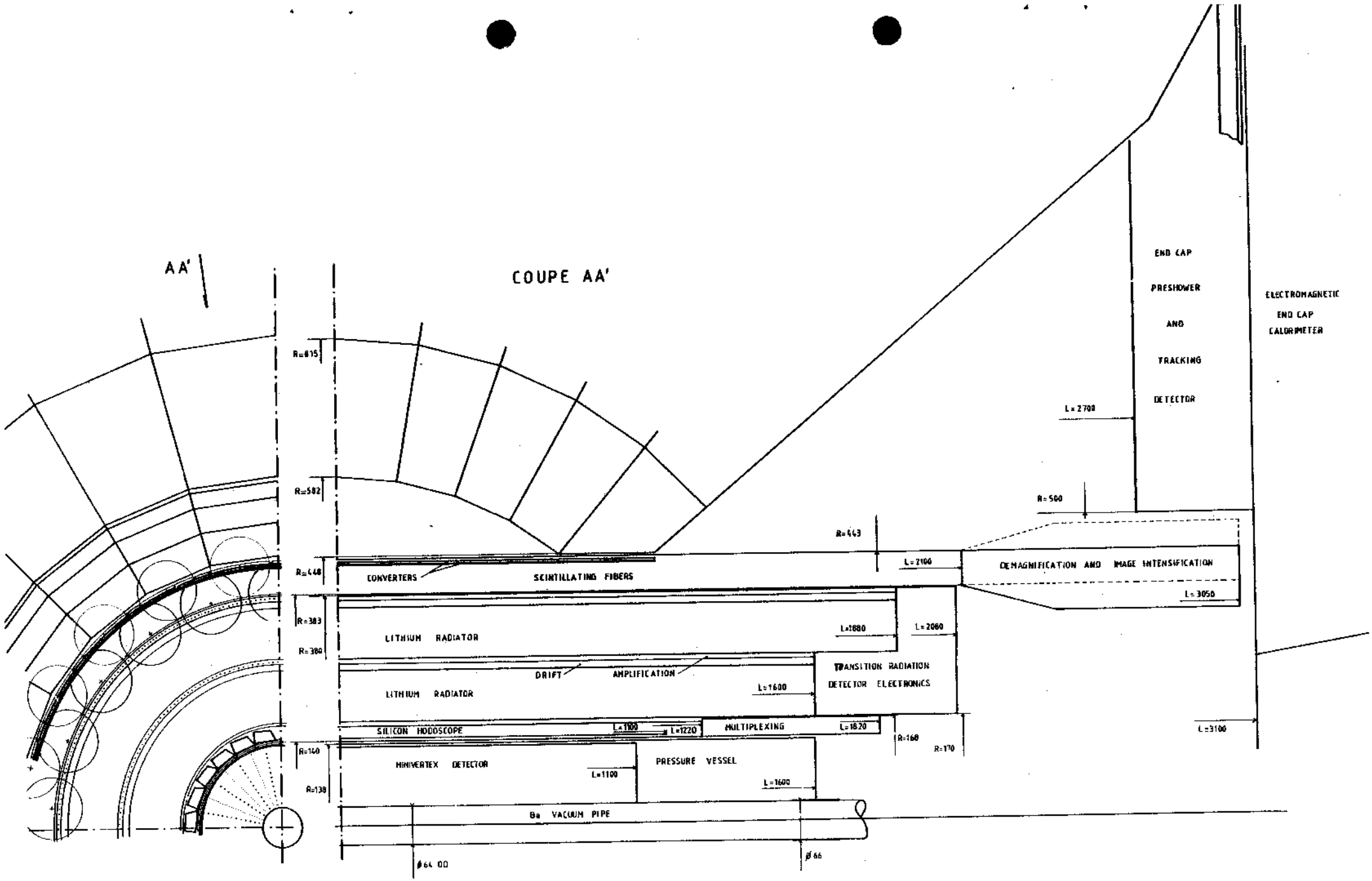
AA'
COUPE AA'
R=615
R=582
R=448
R=383
R=380
R=140
R=138
CONVERTERS
SCINTILLATING FIBERS
LITHIUM RADIATOR
LITHIUM RADIATOR
DRIFT
AMPLIFICATION
SILICON HODOSCOPE
L=1100
L=1220
MULTIPLEXING
L=1820
HNIVERTEX DETECTOR
L=1100
PRESSURE VESSEL
L=1600
Be VACUUM PIPE
ϕ64.00
ϕ66
L=1600
L=1680
L=2060
TRANSITION RADIATION
DETECTOR ELECTRONICS
R=160
R=170
R=443
L=2100
DEMAGNIFICATION AND IMAGE INTENSIFICATION
L=3050
R=500
L=2700
END CAP
PRESHOWER
AND
TRACKING
DETECTOR
ELECTROMAGNETIC
END CAP
CALORIMETER
L=3100

Fig. 1

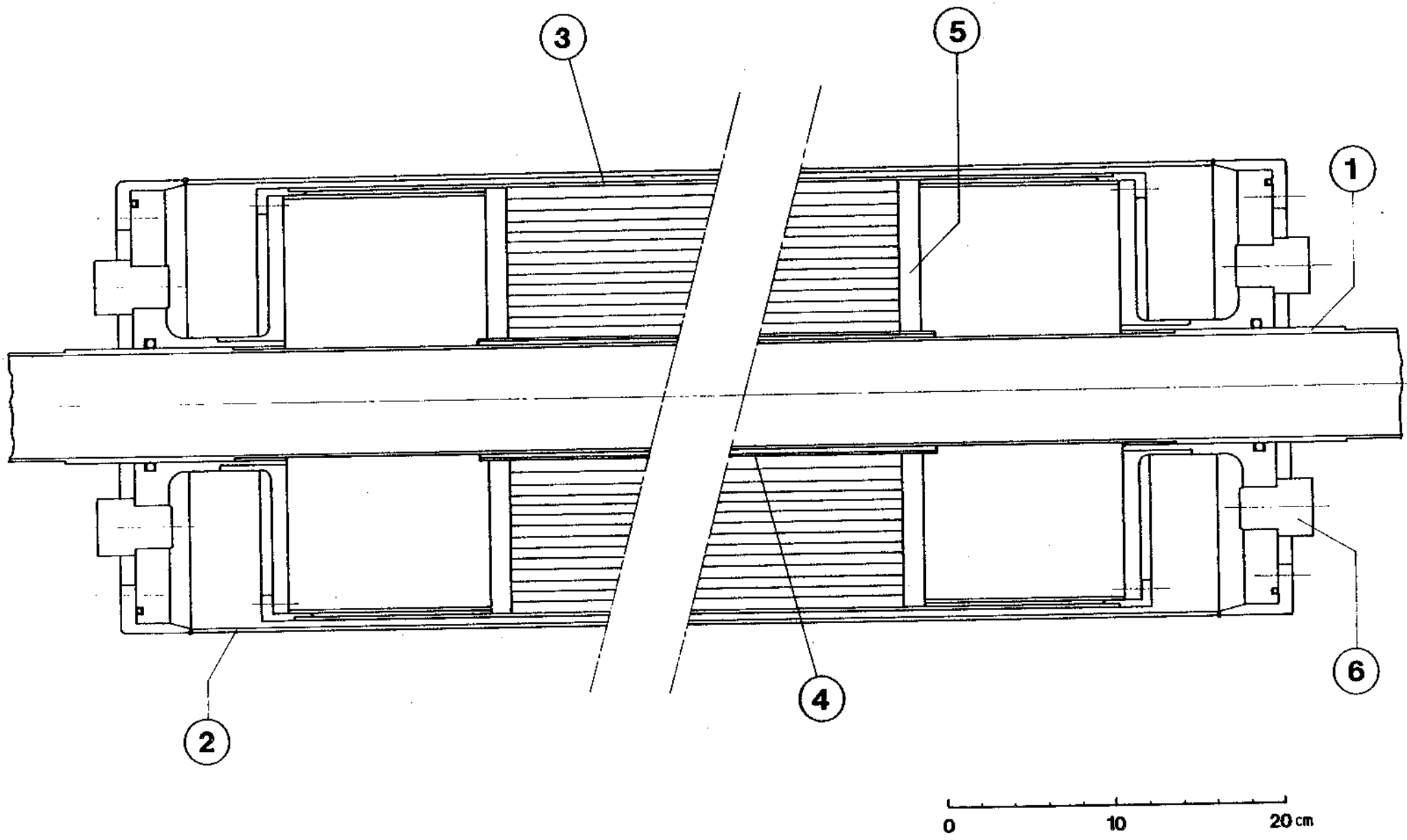

Fig. 2

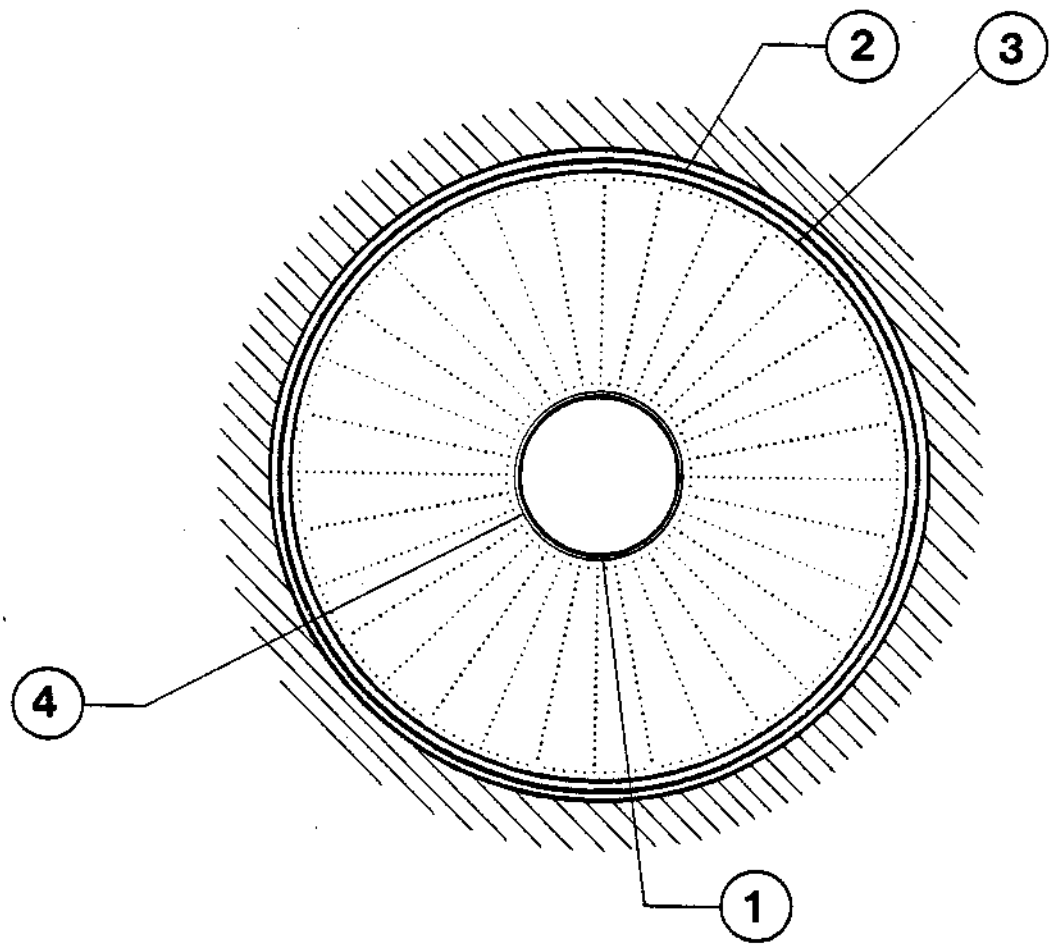

Fig. 3

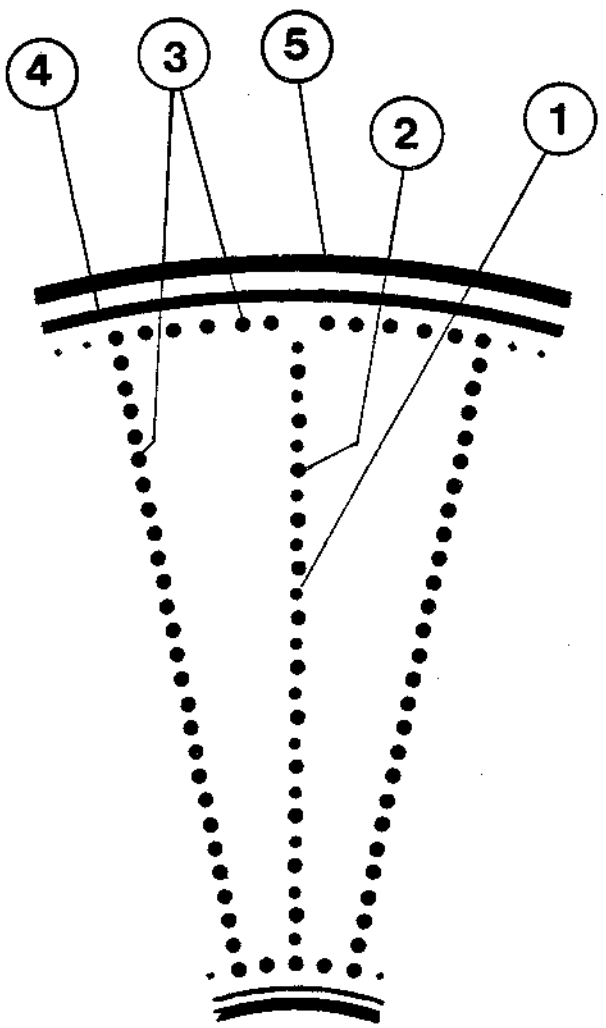

Fig. 4

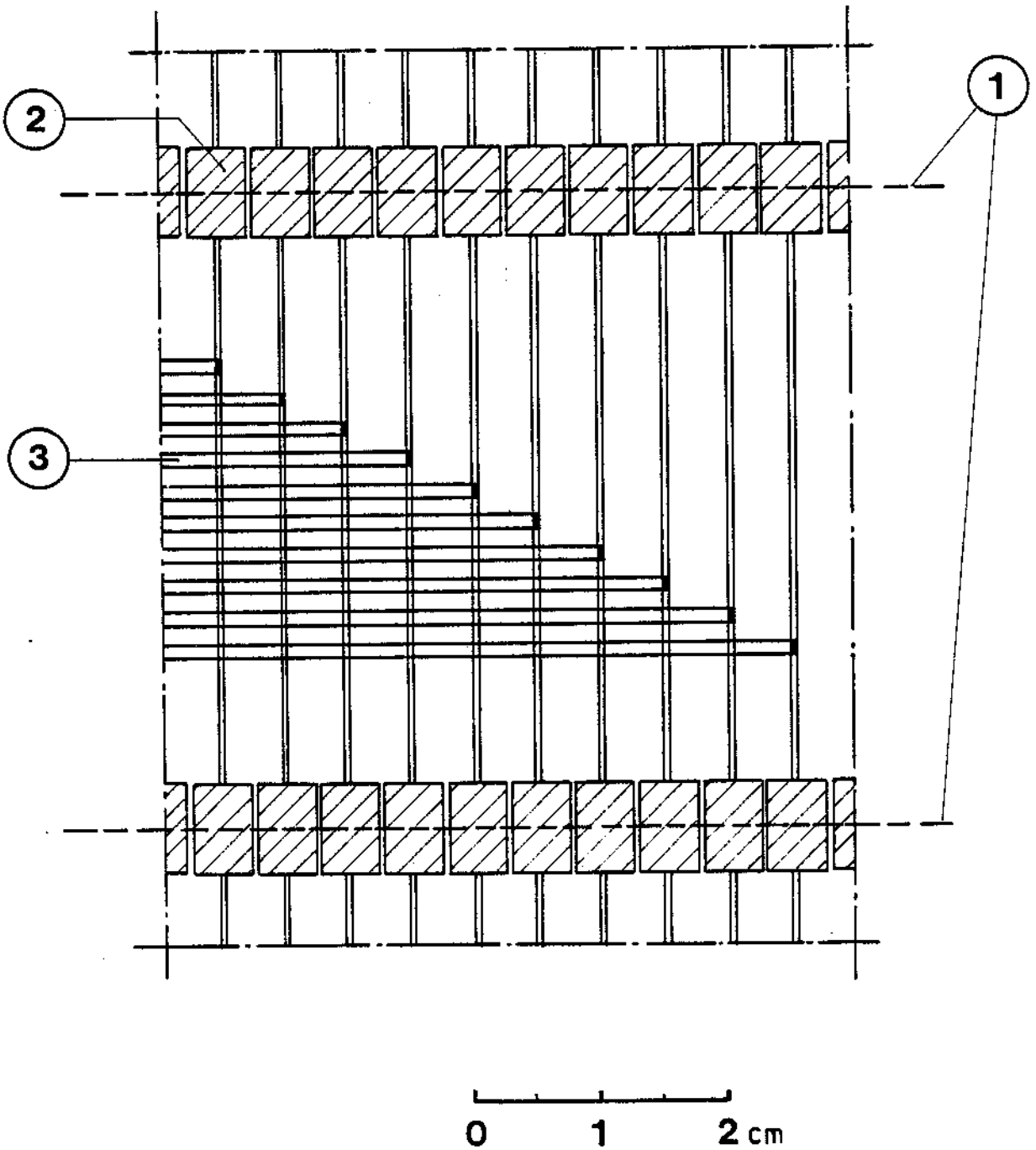

Fig. 5

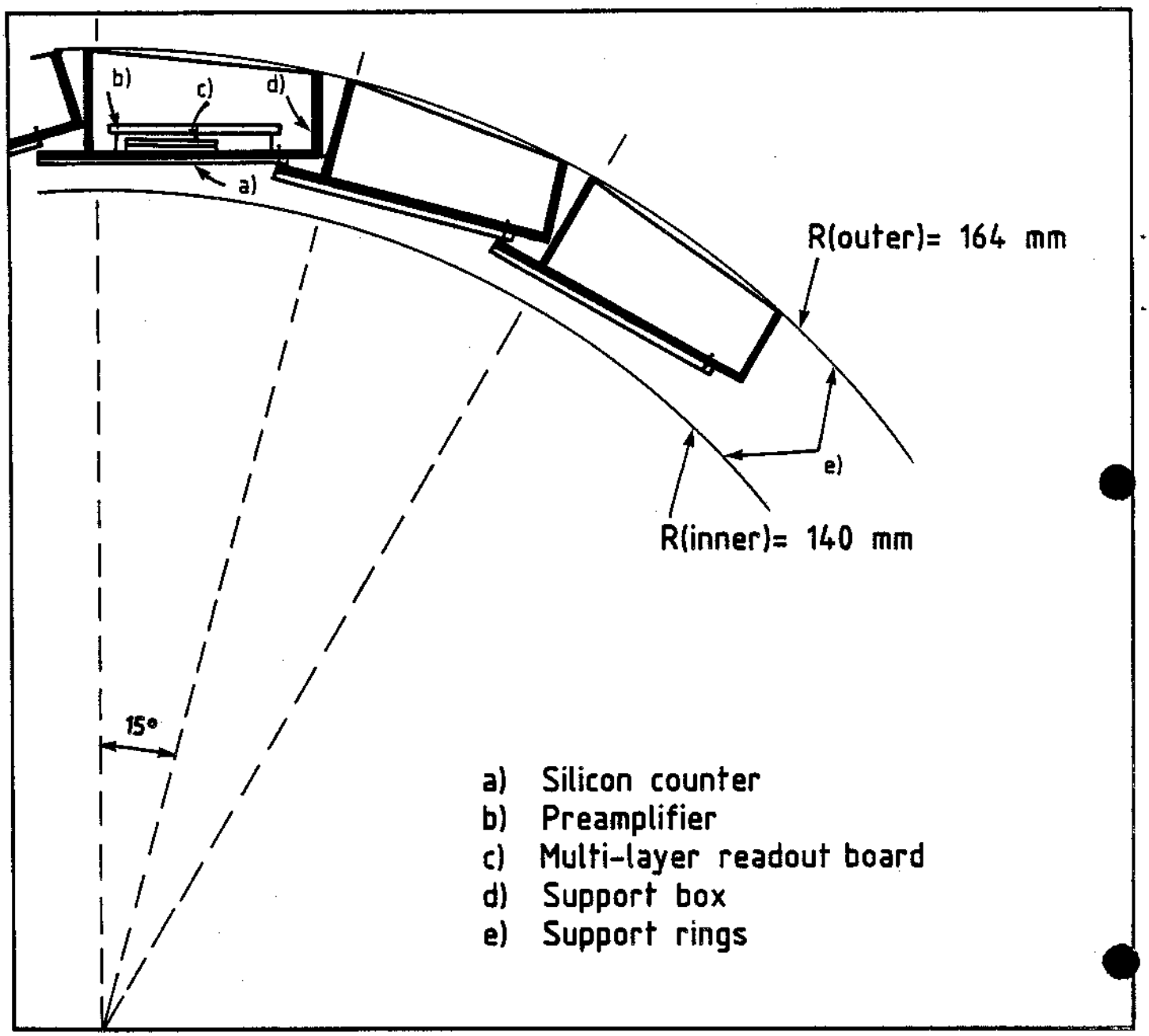
b)
c)
d)
a)
R(outer)= 164 mm
e)
R(inner)= 140 mm
15°
a) Silicon counter
b) Preamplifier
c) Multi-layer readout board
d) Support box
e) Support rings

Fig. 6

a)

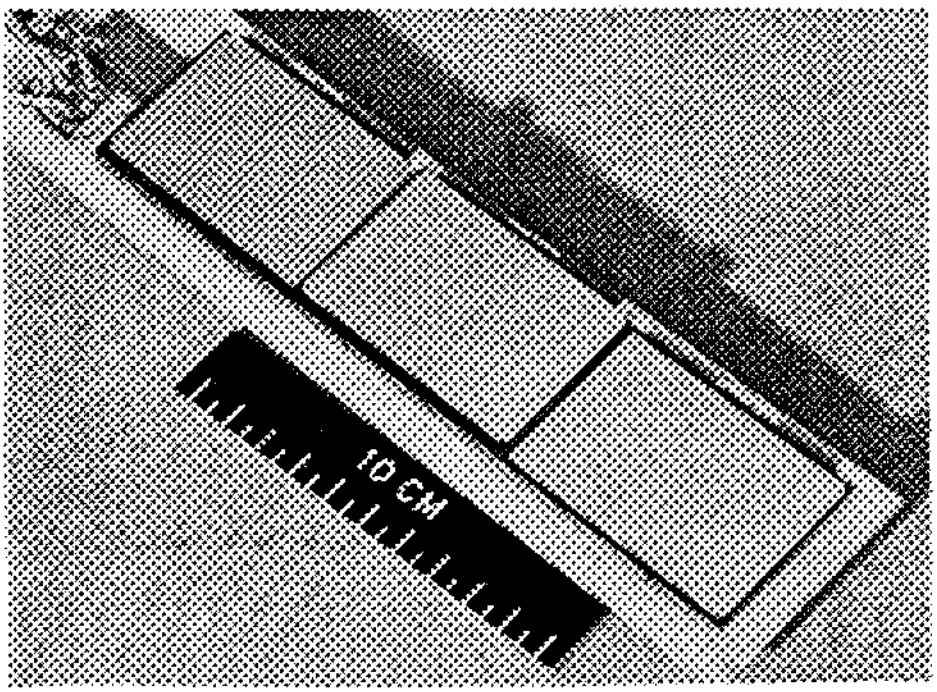

b)

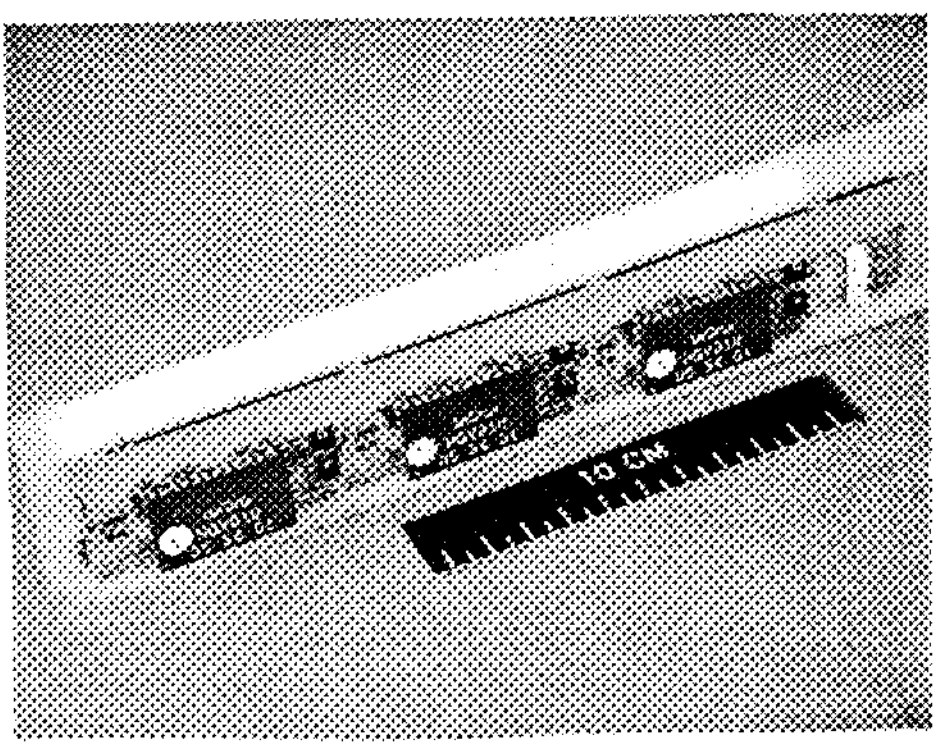

Fig. 7

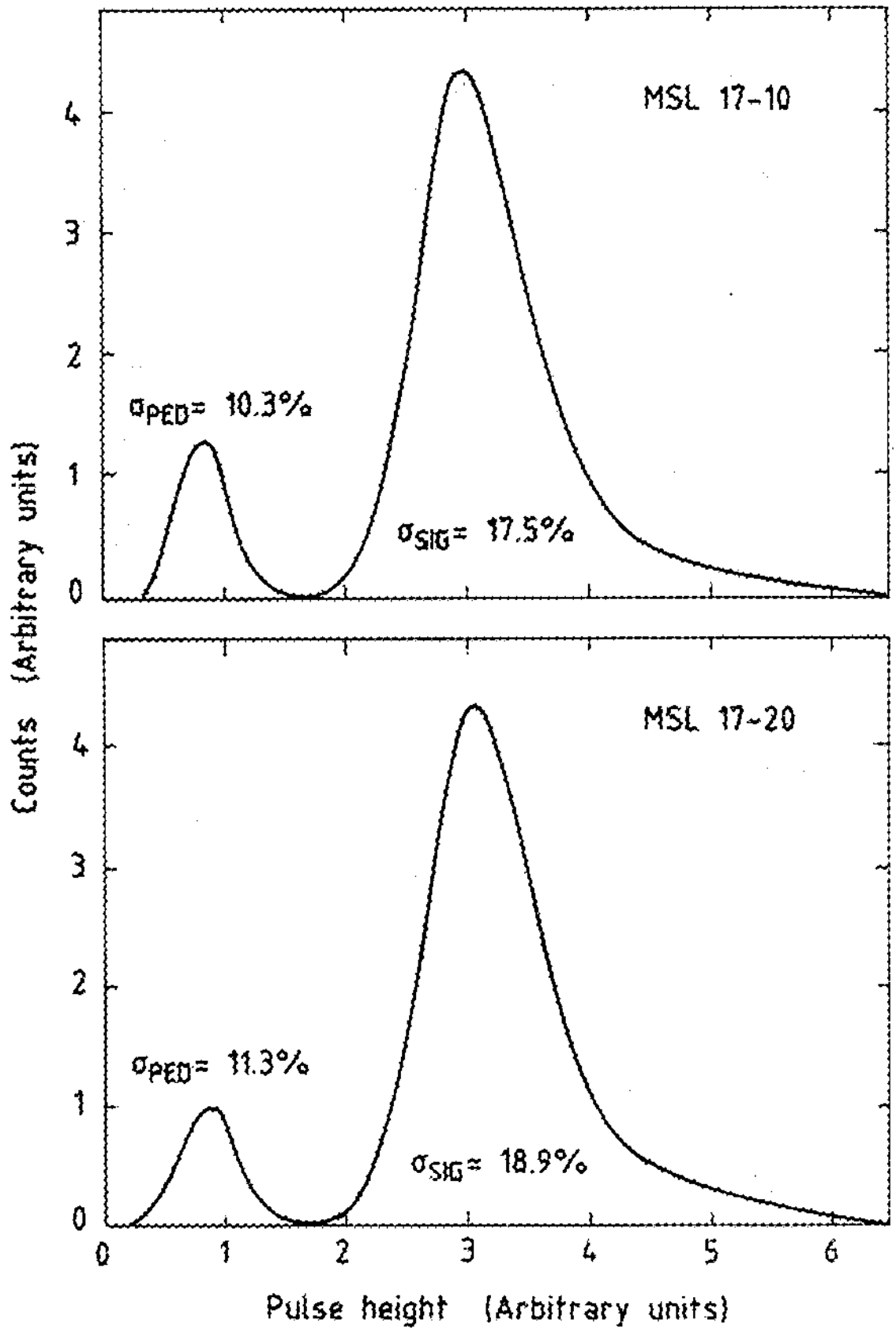
MSL 17-10
σPED= 10.3%
σSIG= 17.5%
MSL 17-20
σPED= 11.3%
σSIG= 18.9%
Counts (Arbitrary units)
Pulse height (Arbitrary units)
0
1
2
3
4
5
6

Fig. 8

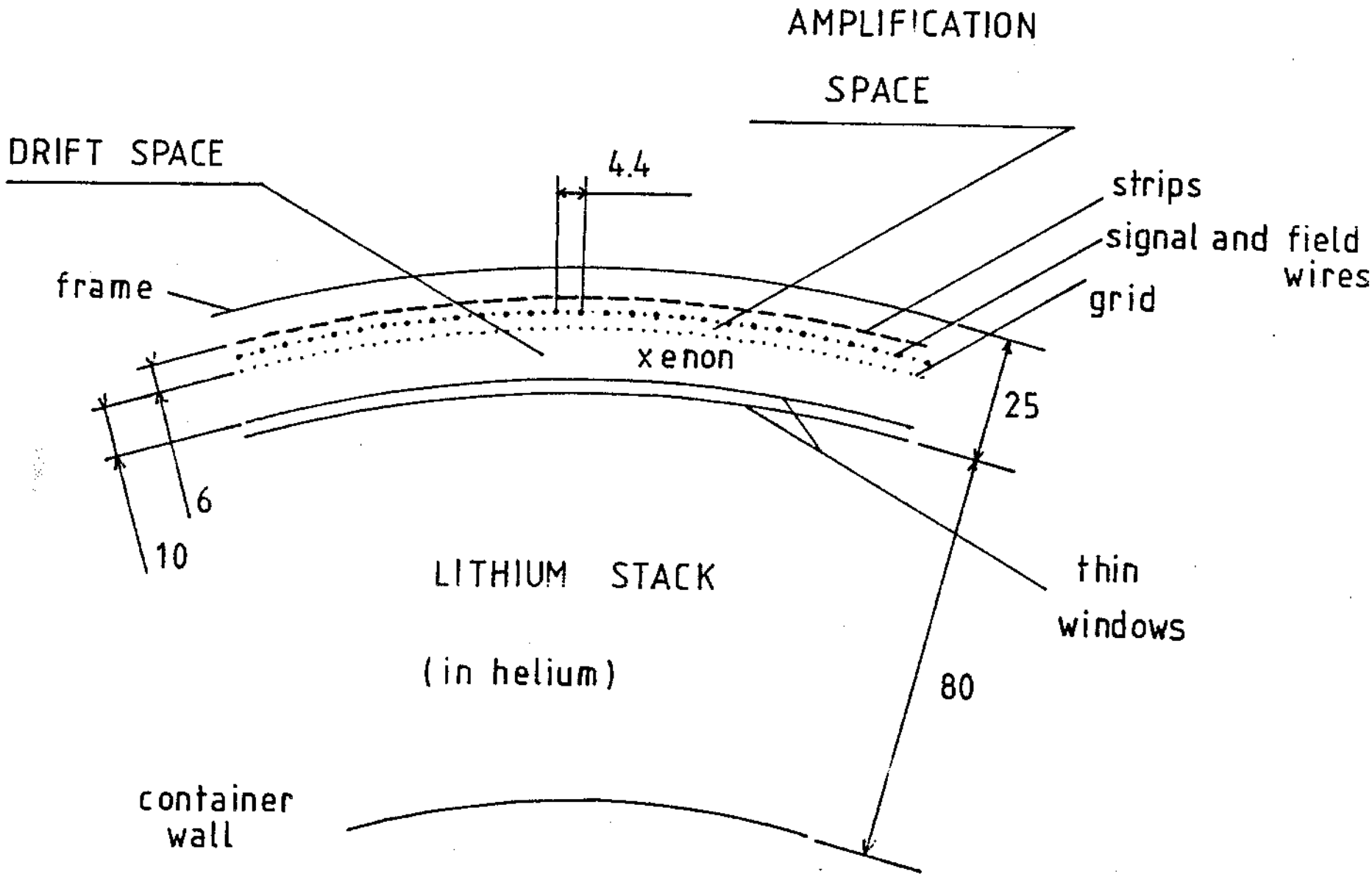
AMPLIFICATION
SPACE
DRIFT SPACE
4.4
strips
signal and field
wires
grid
frame
xenon
25
6
10
LITHIUM STACK
(in helium)
thin
windows
80
container
wall

Fig. 9

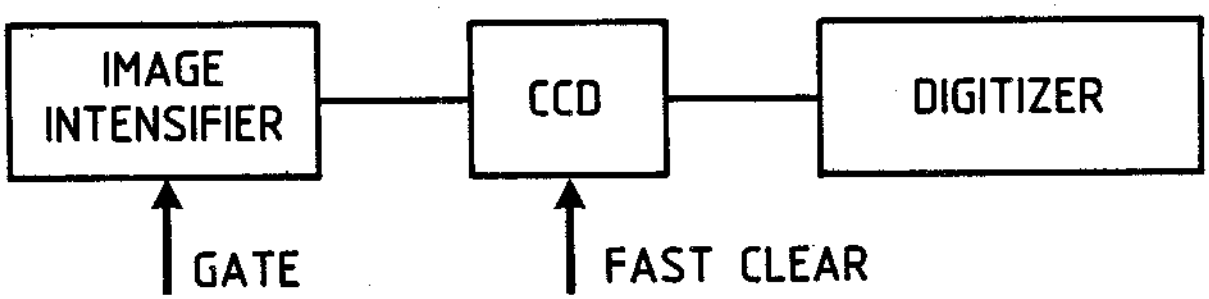
IMAGE
INTENSIFIER
CCD
DIGITIZER
GATE
FAST CLEAR

Fig. 10

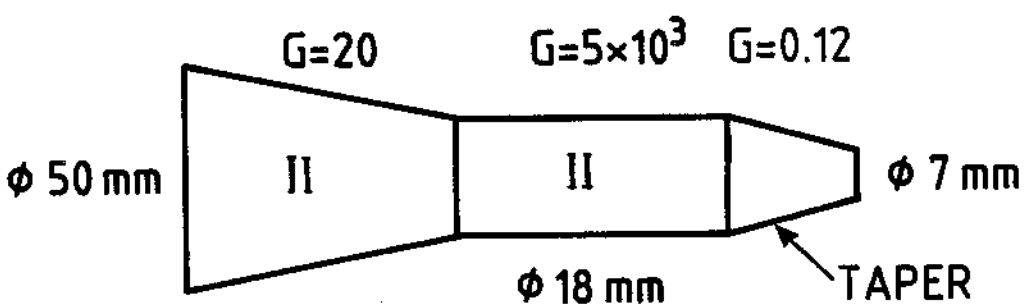
G=20
G=5×10³
G=0.12
ϕ 50 mm
II
II
ϕ 7 mm
ϕ 18 mm
TAPER

Fig. 11